2020-05

Effects of fullerene C60 in blue mussels: Role of mTOR in autophagy related cellular/tissue alterations

Sforzini, S

10.1016/j.chemosphere.2019.125707
Chemosphere
Elsevier BV

Effects of fullerene C_{60} in blue mussels: role of mTOR in autophagy related cellular/tissue alterations

Susanna Sforzini [a], Caterina Oliveri [a], Audrey Barranger [b], Awadhesh N. Jha [b], Mohamed Banni [c], Michael N. Moore [b, d, e], Aldo Viarengo [f]

[a] Department of Sciences and Technological Innovation (DiSIT), University of Piemonte Orientale "A. Avogadro", V.le T. Michel 11, 15121 Alessandria, Italy

[b] School of Biological and Marine Sciences, University of Plymouth, Drake Circus, Plymouth, PL4 8AA, UK

[c] Laboratory of Biochemistry and Environmental Toxicology, ISA, Chott-Mariem, Sousse, Tunisia

[d] European Centre for Environment & Human Health (ECEHH), University of Exeter Medical School, Truro, TR1 3HD, UK

[e] Plymouth Marine Laboratory, Plymouth, PL1 3DH, UK

[f] Institute for the study of Anthropic impacts and Sustainability in marine environment - National research Council (CNR-IAS), Via de Marini 6, 16149 Genova, Italy

Corresponding author:

Aldo Viarengo

IAS-CNR

Via De Marini 6, 16149 Genova, Italy

Phone: +393357182939

E-mail: aldo.viarengo@ias.cnr.it

Abstract

The effects of C_{60} on mTOR (mechanistic Target of Rapamycin) activity in mussel digestive gland were investigated. mTOR is a kinase that senses physiological and environmental signals to control eukaryotic cell growth. mTOR is present in two complexes: the phosphorylated mTORC1 regulates cell growth by activating anabolic processes, and by inhibiting catabolic processes (i.e. autophagy); mTORC2 also modulates actin cytoskeleton organization. Mussels were exposed to C_{60} (0.01, 0.1 and 1 mg/L) for 72h. Immunocytochemical analysis using a specific antibody revealed the cellular distribution of C_{60} in mussel digestive gland, already at the lowest concentration. In exposed mussels, the dephosphorylation of mTORC1 and mTORC2 may explain the C_{60} effects, i.e. the reduction of lysosomal membrane stability, the enhancement of LC3B protein, and the increase of lysosomal/cytoplasmic volume ratio; as well the cytoskeletal alterations. No oxidative stress was observed. Multivariate analysis was used to facilitate the interpretation of the biomarker data. Finally, a low density oligo-microarray was used to understand the cellular responses to fullerene. Transcriptomics identified a number of differentially expressed genes (DEGs) showing a maximum in animals exposed to 0.1 mg/L C_{60}. The most affected processes are associated with energy metabolism, lysosomal activity and cytoskeleton organization. In this study, we report the first data on the subcellular distribution of C_{60} in mussel's cells; and on the involvement of mTOR inhibition in the alterations due to nanoparticle accumulation. Overall, mTOR deregulation, by affecting protein synthesis, energy metabolism and autophagy, may reduce the capacity of the organisms to effectively grow and reproduce.

Keywords: mussel, mTOR, fullerene C_{60}, autophagy, cytoskeleton, transcriptomics

1. Introduction

The fullerenes represent one major class of carbon-based nanoparticles (NPs) (Khan et al., 2017) that exist naturally (e.g. in geological materials), are generated incidentally (e.g. from combustion processes) and are produced in large quantities as engineered nanomaterials (Buseck et al., 1992; Nielsen et al., 2008). Fullerenes are widespread in all ecosystems (surface waters -Emke et al., 2015 and Farré et al. 2010; atmospheric aerosols -Sanchís et al., 2012; soils -Sanchís et al. 2013; sediments -Sanchís et al. 2015) and, with the further development of nanotechnology, their environmental concentration is continuously increasing (Benn et al., 2012; Pycke et al., 2012). There is however lack of information with respect to mechanisms of actions of these materials for hazard and risk assessment, in particular, in the marine environment.

In the fullerene family, C_{60} (buckminsterfullerene) is the most abundant representative. Its unique characteristics render C_{60} and its derivatives promising candidates for various applications in different fields such as medicine and electronics (Urbaszek et al., 2017).

C_{60} has been demonstrated to act as a “free radical sponge” with an antioxidant efficacy hundreds of times greater than conventional antioxidants (Krusic et al., 1991; Liu et al., 2014). However, somewhat paradoxically, C_{60} is also able to generate reactive oxygen species (ROS) by light excitation (Trpkovic et al., 2012). This dual property of fullerene C_{60} (both pristine as well derivatized) molecules, and their bioaccumulation capacity, have given rise to numerous studies aimed at clarifying whether these particles may represent a risk to animal and human health (Goodarzi et al., 2017; Trpkovic et al., 2012).

Studies about the toxicity of fullerene toward vertebrates and invertebrates has highlighted that these particles exert ROS-mediated and/or ROS-independent adverse effects depending on various factors (e.g. physicochemical properties, target cells and tissues, type of exposure) (Canesi et al., 2010; Goodarzi et al., 2017; Oberdörster, 2004; Ringwood et al., 2009; Trpkovic et al., 2012). Although the modes of toxic action are not yet fully understood, several studies have indicated

induction and perturbation of autophagy as an emerging mechanism of fullerene (and more in general of nanomaterials) cellular pathophysiology (Stern et al., 2012; Zabirnyk et al., 2007). Many studies have demonstrated nanomaterial-induced lysosomal dysfunctions (Stern et al., 2012). In particular, fullerene was shown to induce a reduction of lysosomal membrane stability (LMS) in marine bivalve molluscs, which are organisms widely used in environmental biomonitoring (Canesi et al., 2010; Dallarés et al., 2018; Maisano et al., 2017; Moore et al., 2009; Ringwood et al., 2009; Sanchís et al., 2018; Viarengo et al., 2007). Destabilisation of lysosomal membranes represents a cellular pathological reaction known to be linked to both augmented and dysfunctional autophagy (Moore et al, 2006).

Macroautophagy is an essential, conserved process that results in the degradation of cytoplasmic components (protein aggregates, organelles, etc.) in lysosomes (Cuervo, 2004; Klionsky and Emr, 2000). Autophagy, both macro- and microautophagy, is crucial for cell homeostasis and survival under both normal and stress conditions; as well is implicated in many relevant diseases (Levine and Kroemer, 2008). One of the key regulators of autophagy is mTOR (mechanistic Target of Rapamycin), an evolutionarily conserved serine/threonine kinase that plays a pivotal role in the regulation of cell growth and metabolism in response to different stimuli, such as nutrients, hormones and stressors (Dobashi et al., 2011; Huang and Fingar, 2014; Saxton and Sabatini, 2017; Soulard et al., 2009).

The aim of this research was to study the effects of C_{60} on mTOR activity and related lysosomal perturbations in the digestive gland or hepatopancreas of blue mussels (*M. galloprovincialis* Lam). mTOR exists in two functionally distinct complexes: namely mTOR complex 1 (mTORC1) and mTOR complex 2 (mTORC2) (Copp et al., 2009; Wullschleger et al., 2006). In particular, the phosphorylated form of mTORC1 regulates cell growth by activating anabolic processes (i.e. transcription, ribosome biogenesis, protein synthesis, etc.), and by inhibiting catabolic processes (such as autophagy); mTORC2 also modulates actin cytoskeleton organization (Saxton and

Sabatini, 2017; Soulard et al., 2009). Tissue C_{60} intracellular accumulation and subcellular distributions were evaluated by immunofluorescence using a specific antibody. Changes in the phosphorylation of mTOR were investigated by an immunocytochemical approach. To study the possible consequences of mTOR dephosphorylation on digestive gland physiology, we analysed LMS and the expression of the protein LC3B (as biomarkers of the autophagic process), lysosomal/cytoplasmic (L/C) volume ratio (revealing excessive levels of autophagy), lysosomal neutral lipid (mainly triglyceride) accumulation (index of lipid metabolic disorders) and lipofuscin accumulation (oxidative stress biomarker); while the changes in cytoskeletal actin/tubulin structures were also evaluated. Previous studies have shown that for lysosomal/autophagic and oxidative stress biomarker data, Principal Component Analysis (PCA) coupled with Hierarchical Cluster Analysis can be used as an indicator of homeostasis or health in cellular systems (Moore, 2010; Moore et al., 2015; Sforzini et al., 2018a). In this investigation, PCA and cluster analysis were used to integrate multi-biomarker data; and to test this as a potential predictive model for cellular patho-physiological function against functional damage in the lysosomes of mussel hepatopancreatic digestive cells (Sforzini et al., 2018a). Finally, due to the relevance of transcriptomic data to understanding the cellular adaptive responses to environmental stressors, a recently developed and validated low density oligo-microarray (465 genes, suitable to follow 15 stress response pathways) was used (Banni et al., 2017; Sforzini et al., 2018b). Transcription of selected genes was verified by RT-qPCR.

2. Materials and methods

2.1. Chemicals and organisms

Chemicals of analytical grade were purchased from Sigma-Aldrich Co. (UK/Italy), unless otherwise indicated. Adult *Mytilus galloprovincialis* Lam. (45-50 mm) sampled from the intertidal zone at Trebarwith Strand, Cornwall, UK, a relatively pristine reference site (50° 38’ 40" N, 4° 45’ 44" W)

were maintained under laboratory conditions prior to the experiments as described previously by Barranger et al. (2019a,b).

2.2. Experimental design and sampling

After depuration, the mussels were transferred to 2-L glass beakers (containing 1.8 L of seawater) to acclimatize for 48 h. Two mussels were used per beaker. A photoperiod of 12 h light : 12 h dark was maintained throughout the experiment. Seawater oxygenation was provided and the seawater quality monitored as described by Barranger et al. (2019a). Mussels were exposed for 3 days with no water changes to 0.01, 0.1 and 1 mg/L C_{60} (fullerene suspension homogenised by ultrasonication) as described by Barranger et al. (2019a). A total of 26 individuals were used per treatment. After 3-day exposure period, mussel sex was determined (Banni et al., 2017). Digestive glands (DG) from 10 female mussels were processed for immunohistochemical and cyotochemical analysis (Sforzini et al., 2018a) as well for transcriptomics (microarray and qRT-PCR) (Banni et al., 2017). The C_{60} concentrations used in these experiments were selected taking into account previous studies (Al-Subiai et al., 2012; Di et al., 2017; Moore et al., 2009).

2.3. Immunohistochemical analysis

Frozen sections (10 µm) of mussel digestive glands obtained by using a cryostatic microtome (LeicaCM3050) were fixed in paraformaldehyde (PFA) solution (4% PFA in phosphate buffer saline-PBS, pH 7.2, 20 min at 20 ± 1 °C) (Sforzini et al., 2014).

Immunofluorescent anti-C_{60} staining was performed in accordance with the method described by Sforzini et al. (2014). In brief, fixed sections were incubated in a permeabilisation and blocking solution (0.5% Triton X-100, 2% bovine serum albumin-BSA, 0.5% rabbit serum in PBS) for 1 h at 20 ± 1 °C. Sections were rinsed and incubated with the primary antibody (monoclonal mouse anti-Fullerene antibody -Santa Cruz Biotechnology Inc., 1/100 in PBS containing 1% BSA and 0.05%

149 Triton X-100) at 4 °C overnight; then the secondary antibody was applied i.e. polyclonal rabbit to
150 mouse (FITC) (Abcam) (1/100 in 1% BSA and 0.05% Triton X-100 in PBS) for 1 h at 20 ± 1 °C in
151 the dark. After rinsing, sections were stained with DAPI (DNA-specific fluorescent probe) and
152 mounted as described in Sforzini et al. (2014).
153 To reveal the possible accumulation of fullerene in the lysosomes of the digestive gland cells of C_{60}
154 exposed mussels, immunofluorescence colocalization of fullerene and the lysosomal enzyme
155 cathepsin D was performed following essentially the method described in Sforzini et al. (2018a).
156 The investigations related to mTOR alterations induced in mussel digestive gland by fullerene C_{60}
157 involved the immunohistochemical analysis of the level of phosphorylation (activation/inhibition)
158 of mTORC1 and mTORC2 as well the of total amount of mTOR. Taking into consideration the
159 recent findings by Copp et al. (2009) about the different phosphorylation of mTOR when associated
160 with mTORC1 and mTORC2 (specifically, mTORC1 contains mTOR phosphorylated
161 predominantly on S2448, whereas mTORC2 contains mTOR phosphorylated predominantly on
162 S2481), we used two different specific antibodies. The methods for the immunofluorescent anti-
163 phospho- mTORC1 (by using the anti m-TOR phospho S2448 antibody, Abcam), as well mTOR
164 staining are reported in Sforzini et al. (2018a). For the evaluation of the level of
165 activation/inhibition of mTORC2, mussel digestive gland sections, after fixation (as described
166 above) were incubated in a permeabilisation and blocking solution (0.5% Triton X-100, 2% BSA,
167 0.5% goat serum in PBS, 1 h at 20 ± 1 °C) and then with the primary antibody (anti m-TOR
168 (phospho S2481) antibody, Abcam, 1/100 in PBS containing 1% BSA and 0.05% Triton X-100)
169 overnight at 4 °C. Sections were then washed and the secondary antibody was applied, i.e.
170 polyclonal goat to rabbit (Chromeo™ 488) (Abcam) (1/100 in 1% BSA and 0.05% Triton X-100 in
171 PBS) for 1 h at 20 ± 1 °C in the dark. Finally, sections were rinsed in PBS, counterstained with
172 propidium iodide and mounted.

Immunofluorescent anti-LC3B staining, autophagy marker microtubule-associated protein chain 3B, was performed by incubating the sections, after permeabilisation and blocking (0.5% Triton X-100, 2% BSA, 0.5% goat serum in PBS, for 1 h at 20 ± 1 °C), with the primary antibody (rabbit polyclonal to LC3B - Abcam, 1/100 in PBS containing 1% BSA and 0.05% Triton X-100, overnight at 4 °C) and then with the secondary antibody i.e. polyclonal goat to rabbit (Alexa Fluor® 488) (Abcam) (1/100 in 1% BSA and 0.05% Triton X-100 in PBS) for 1 h at 20 ± 1 °C in the dark. After rinsing, sections were stained with DAPI and mounted.

To reveal the potential link between the state of activation/inactivation of mTORC2 and the cytoskeleton structure, immunofluorescent anti-tubulin staining and F-actin staining was performed as described by Banni et al. (2017) and Sforzini et al. (2018b). Antibody to tubulin and F-actin combination staining was also performed: after the reaction for the primary antibody (see Banni et al., 2017), sections were incubated with the secondary antibody i.e. goat anti-rabbit (DyLight® 594) (Abcam) (1/100 in 1% BSA and 0.05% Triton X-100 in PBS) for 1 h at 20 ± 1 °C in the dark; sections were washed in PBS and then incubated with Green Fluorescent Phalloidin Conjugate (CytoPainter F-actin Labeling Kit-Green Fluorescence -Abcam) for 1 h at 20 ± 1 °C. After rinsing, sections were mounted.

Control sections for non-specific staining were processed without the primary or secondary antibodies: no positive stain was observed. Slides were viewed under 400 × magnification by an inverted photo-microscope (Zeiss Axiovert 100M connected to a digital camera Zeiss AxioCam MRm) equipped for fluorescence microscopy using FITC, Rhodamine and DAPI emission filters. Sections double immunolabelled for C_{60} and cathepsin D and for mTOR were viewed under 400 × magnification by Axio Observer and images were taken with ApoTome.2 (Zeiss, Germany). The obtained images were analysed by an image analysis system (Scion Image) for the quantification of the mean fluorescence intensity.

198 *2.4. Lysosomal alterations*

199 A set of parameters was used to evaluate the possible consequences of mTORC1 dephosphorylation
200 induced in mussels by increasing concentrations of fullerene C_{60} on digestive gland cell physiology.
201 The determination of the biomarkers was evaluated on cryostat digestive gland sections (10 µm)
202 obtained as described above. The LMS (based on the latency of the lysosomal enzyme N-acetyl-β-
203 hexosaminidase -NAH) and the L/C volume ratio (in sections reacted for NAH) were assessed as
204 reported by Moore (1976, 1988) and by Moore and Clarke (1982), respectively. The lipofuscin
205 content was determined using the Schmorl reaction (Moore, 1988; Pearse, 1972), and neutral lipid
206 content by the Oil Red-O (ORO) staining (Moore, 1988). Sections were viewed under 400 ×
207 magnification by a Axiolab photo-microscope and the pictures obtained were analysed using an
208 image analysis system (Scion Image). LMS was expressed as labilization period (min); L/C volume
209 ratio as well lipofuscin and neutral lipid accumulations were expressed as a percentage variation
210 with respect to controls.

211

212 *2.5. Univariate statistical analysis*

213 At least five replicates per control and per C_{60} concentration were analysed. Each replicate consists
214 of the digestive gland from one mussel; the molluscs were sampled from different beakers. The
215 non-parametric Mann-Whitney *U*-test was employed to compare the data from C_{60} exposed
216 organisms with those of the controls ones.

217

218 *2.6. Multivariate statistical analysis*

219 Biomarker data for mussels treated with C_{60} fullerene were analysed using non-parametric
220 multivariate analysis software, PRIMER v 6 (PRIMER-E Ltd., University of Aukland, New
221 Zealand; Clarke, 1999; Clarke & Warwick, 2001). All of the biomarker data were log transformed
222 [$\log_n(1+x)$] and standardised to the same scale. Principal component analysis (PCA) and

hierarchical cluster analysis, derived from Euclidean distance similarity matrices were used to visualise dissimilarities between sample groups. The results were further tested for significance using non-parametric analysis of similarity (PRIMER v6 - ANOSIM), which is an approximate analogue of the univariate ANOVA and reflects on differences between treatment groups in contrast to differences among replicates within samples (the *R* statistic). Under the null hypothesis H_0 ("no difference between samples"), $R = 0$, and this was tested by a non-parametric permutations approach. Using this approach, there should be little or no effect on the average R value if the labels identifying which replicates belong to which samples are randomly rearranged.

Finally, correlation coefficients for the individual biomarkers comprising the first principal component PC1 (representing integrated biomarker data) for the various experimental treatments were derived, including that for lysosomal membrane stability, which has been used previously as an integrated measure of cellular well-being (Allen and Moore, 2004; Moore et al., 2006; Sforzini et al., 2015, 2017, 2018a).

2.7. RNA isolation and Microarray hybridization

Total RNA was prepared from a digestive gland tissues according to Chomczynski and Sacchi (1987), using TRI-Reagent. A total number of 5 biological replicates (pools made of two mussels each) were considered. 5 µg of total RNA from each pool was reverse transcribed using oligodT(19)VN primer (Banni et al., 2011). Competitive dual-color microarray hybridization was carried out using the new STREM platform (Banni et al. 2017; Barranger et al., 2019b). All the procedure was conducted according to Banni et al. (2017) and Barranger et al. (2019b). Global mean normalization and Log_2 transformation was performed for each expression level as described in Banni et al. (2017). DEGs were identified by Significance Analysis of Microarray (SAM, http://statweb.stanford.edu/~tibs/SAM/).

248 *2.8. qRT-PCR*

249 The qRT-PCR reactions were realised using the same RNA extract as microarray hybridization.
250 Four probes and primer pairs (tubulin, tripsin, catalase and cytosolic superoxide dismutase Table S1
251 - see Supplementary Information) were employed. The cDNA preparation and the Q-PCR details
252 are as described elsewhere in details (Banni et al., 2011, 2017; Barranger et al., 2019b; Negri et al.,
253 2013). The relative expression data were normalized against ribosomal protein riboL27
254 (AJ625928), an invariant actin isotype (AJ625116), and 18S rRNA (L33452). Statistical analyses
255 were performed on the group mean values using a random reallocation test (Pfaffl et al., 2002).
256

257 ## 3. Results

258 *3.1. Immunohistochemical and cytochemical analysis*

259 The concentrations of C_{60} utilised in this study did not provoke any mortality (data not shown) in
260 *M. galloprovincialis* after 3 d of exposure; the results demonstrate that C_{60} accumulated in the
261 digestive gland of molluscs induced, even at the lowest dose, significant changes of mTOR
262 activation with negative consequences on cellular and tissue physiology (Fig. 1-4).
263 Western blot (WB) is often used as a complementary assay to confirm antibody specificity in
264 immunohistochemistry (IHC) and provide more quantitative analysis of protein levels. However,
265 the epitope recognized by the primary antibody may not be identically available in WB and IHC
266 assays (www.cellsignal.co.uk); in the case of phosphoproteins (as mTOR), the phosphate could be
267 hydrolysed by phosphatases released during the sample preparation. For these reasons, in this study,
268 we decided to use immunohistochemistry to evaluate by specific antibodies the protein
269 expression/level of phosphorylation in cryostat sections that are suitable for maintaining the cellular
270 characteristics and the structure of native proteins.
271 Immunohistochemical analysis of digestive gland sections of mussels exposed to C_{60} using a
272 specific anti-fullerene antibody showed a positive reaction (Fig. 1B-D); no staining was observed in

control animals (Fig. 1A). Co-localization of fullerene and the lysosomal enzyme cathepsin D by double immunofluorescence labelling demonstrated the accumulation of C_{60} inside lysosomes (Fig. 1F). Quantification of the C_{60} fluorescence signal by digital imaging (Fig. 1E) showed a significant increase in fluorescence intensity in mussels exposed to all the concentrations, with respect to controls; and a plateau was reached at the lowest dose (10 µg/L). No statistically significant difference was observed among the different C_{60} concentrations.

Immunofluorescence labelling of mussel digestive gland sections with the two different antibodies to phospho-mTOR (phosphorylated on S2448 -mTORC1, and on S2481 -mTORC2) was positive in control animals (Fig. 2A, panels 1, 2). The respective signals were differentially located, mainly in the perinuclear region of the tubule epithelial cells for mTORC1 (Fig. 2E, panel 1); and generally in the cytoplasm for mTORC2 (Fig. 2E, panel 2). The immunocytochemical data demonstrated that all the different concentrations of C_{60} induced a strong dephosphorylation of mTOR (for both S2448 and S2481), with respect to the controls (Fig. 2B, C, D, F - panels 1, 2). When the digestive gland tissue sections were reacted for the mTOR antibody in order to reveal the protein level, the fluorescent signal in C_{60} exposed mussels showed no change when compared to controls (Fig. S1 – see Supplementary Information); as for phospho-mTOR, similar values were obtained in animals exposed to all the different concentrations (Fig. S1 E).

The strong inactivation (dephosphorylation) of mTOR was accompanied by pathological reactions involving the lysosomal vacuolar system, as well by cytoskeleton structural alterations. In particular, C_{60}, already at the lowest concentration (0.01 mg/L), induced a strong decrease of LMS in digestive gland cells (Fig. 3A), associated with an increase in the expression of the protein LC3 (autophagy marker microtubule-associated protein chain 3B - LC3B) (Fig. 3C); a significant enhancement of L/C volume ratio, revealing an injury at the cell and tissue level, was also observed (+ 49%, with respect to controls) (Fig. 3B). Fullerene caused an alteration of fatty acid metabolism in mussels: we found in the lysosomes a significant accumulation (lipidosis) of neutral lipids, which

was greater at the lowest concentration (0.01 mg/L) (+ 84%, with respect to controls) (Fig. 3D). However, no oxidative stress was generated in the digestive gland cells of C_{60} exposed mussels, as demonstrated by the results of lysosomal lipofuscin content, which showed no change compared to the controls (Fig. 3E). The investigations related to the possible negative consequences of C_{60} exposure on the cytoskeleton involved the immunofluorescent analysis of tubulin, as well the fluorescent staining of F-actin. As shown in Fig. 4, both of these cytoskeletal components presented strong alterations in mussels exposed at all the different C_{60} concentrations. In particular, even at the lowest dose (10 µg/L), a rearrangement was observed of the tubulin structure, with the presence of highly stained cytoplasmic granules containing the protein. When the digestive gland sections were stained for F-actin, in C_{60} exposed mussels the cytoskeletal architecture of the digestive tubules was strongly affected, with the alterations in the actin component of the cytoskeleton being particularly evident in the cortical compartment of the cells.

3.2. Multivariate analysis of biomarker reactions

Principal component (PCA) and hierarchical cluster analysis of all the biomarker reactions showed that C_{60} had a significant detrimental effect on the digestive cells of mussels (Fig. 5); and that the first principal component (PC1) captured 69.6% of the variation. Analysis of similarity shows that the controls were significantly different from the treatments (ANOSIM, global R Statistic: $R = 0.512$, $P \leq 0.01$). Treatments with the three concentrations of C_{60} were clearly separated from the control ($P < 0.01$). Only C_{60} 0.01 mg/L and C_{60} 0.1 mg/L showed a significant difference within the C_{60} treatments ($P < 0.05$; Fig. 5). Table 1 shows that some of the correlation coefficients in the linear combinations of biomarkers making up PC1 were statistically significant, including lysosomal membrane stability, lysosomal lipid, phosphorylated mTORC1 (p-mTORC1 active form) and lysosomal-cytoplasmic volume ratio.

323 *3.3. Transcriptomic analysis*

324 In order to compare the expression patterns of genes in response to increasing fullerene
325 concentrations compared to controls, a cDNA microarray with available annotated gene sequences
326 from *M. californianus*, *M. galloprovincialis*, *M. edulis*, and *C. gigas* containing 465 probes was
327 used. Based on the enriched GO functional annotation, target genes were selected to explore 6
328 distinct biological processes related to the stress response in bivalve molluscs, including translation,
329 carbohydrate metabolism, mitochondrial activities, lysosomal activity, proteolysis and cytoskeletal
330 organisation. Transcriptomic analysis identified a number of DEGs (differentially expressed genes)
331 showing a maximum of 87 DEGs in animals exposed to 0.1 mg/L C_{60} (Table 2; Figure 6). The
332 resulting expression profiles identified a total of 113 differentially expressed genes (DEGs) in at
333 least one condition (Fig. 6). Of the 113 DEGs, 28 genes were found to be in common in the three
334 experimental conditions. Comparative analysis showed differences in gene expression level in
335 mussels exposed to 0.1 mg/L C_{60} with the maximum DEGs number related to translation and
336 cytoskeletal organization (Fig. 7).

337

338 *3.4. Confirmation analysis*

339 We performed a qRT-PCR to refine and confirm the relative expression levels of four genes
340 belonging to the most important biological processes, including the genes encoding trypsin
341 (proteolysis), tubulin (cytoskeleton), catalase and cytosolic superoxide dismutase (oxidative stress).
342 Microarray and qRT-PCR data indicated a positive relationship in all cases (Fig. S2, see
343 Supplementary Information).

344

345 ## 4. Discussion

346 The effects of fullerene C_{60} on mTOR (mechanistic target of rapamycin) were investigated with
347 particular emphasis on the potential consequences of its deregulation on intracellular lysosomal

348 autophagy in digestive gland/hepatopancreatic cells in blue mussels (*M. galloprovincialis*). The
349 digestive gland was chosen for the analysis as it is the organ devoted to food absorption and
350 digestion (Bayne, 2009); as well to the accumulation and detoxification of toxic contaminants (Al-
351 Subiai et al., 2012; Banni et al., 2016; Barranger et al., 2019a,b; Di et al., 2017; Gomes et al., 2012;
352 Moore et al., 2007; Sforzini et al., 2018a,b; Viarengo et al., 1981). Moreover, digestive gland has
353 been identified as a relevant target for nanoparticle accumulation and effects (Al-Subiai et al., 2012;
354 Barranger et al., 2019a,b; Canesi et al., 2012; Di et al., 2017; McCarthy et al., 2013; Tedesco et al.,
355 2010).
356 Fullerene C_{60} uptake and distribution have been shown *in vitro* on various cell types using various
357 methods (e.g. TEM/EFTEM techniques, by synthesizing fluorescent labelled fullerene, by
358 immunostaining - Franskevych et al., 2017; Grebinyk et al., 2018; Porter et al., 2007; Raoof et al.,
359 2012; Ringwood et al., 2009; Russ et al., 2016). *In vivo* studies have largely focused on identifying
360 the uptake capacity of different organs and tissues (Bullard-Dillard et al., 1996; Sumner et al., 2015;
361 Tervonen et al., 2010). To the best of our knowledge, this is the first study that demonstrated the *in*
362 *vivo* intracellular accumulation and the subcellular distribution of C_{60} in tissue sections of fullerene
363 exposed organisms. The immunocytochemical analysis, using a specific anti-fullerene C_{60} antibody,
364 enabled the localisation of C_{60} in the digestive tubule epithelial cells; while the double fluorescent
365 labelling with the antibody against cathepsin D (a highly conserved lysosomal protease; Phillips et
366 al., 2006) showed that fullerene is actually sequestered in secondary lysosomes. Rather
367 unexpectedly, immunofluorescence data showed that the maximum uptake of $C_{60}$was achieved in
368 mussels exposed at the lowest concentration (10 µg/L). Immunofluorescent anti-C_{60} staining
369 reaction was performed following a methodology (recently developed by Sforzini et al., 2014) that
370 allows the localization of contaminants (such as B[*a*]P and TCDD) within tissues of animals
371 exposed to low chemical concentrations (Banni et al., 2016; Sforzini et al., 2018a, 2018b).
372 Chemical analytical results for the molluscan digestive glands, sampled in the same experiment

(Barranger et al., 2019), are fully supportive of the immunocytochemical fluorescence analysis. Fullerene accumulated in the digestive gland of C_{60} treated mussels did not show any significant change among the different doses (0.01, 0.1, 1 mg/L). Previously reported investigations have clearly demonstrated that in mussels exposed to 0.1 and 1 mg/L C_{60}, the digestive gland represents a relevant site of chemical accumulation (Al-Subiai et al., 2012; Di et al., 2017).

Fullerene exposure caused a marked inhibition of mTOR. This serine/threonine protein kinase plays an essential role in regulating cell growth and division in response to various factors such as nutrients, hormones and environmental stressors (Dobashi et al., 2011; Huang and Fingar, 2014; Saxton and Sabatini, 2017; Soulard et al., 2009). mTOR is found in two distinct evolutionarily conserved signalling complexes: mTOR complex 1 (mTORC1) regulates cell growth and metabolism; and mTOR complex 2 (mTORC2) also plays a role in the regulation of the actin cytoskeleton organization (Dobashi et al., 2011). The dephosphorylation (inhibition) of mTOR kinase in both mTOR complexes has been shown to cause an enhancement of the autophagic activity, a decrease in protein synthesis, reduced mitochondrial activity (mTORC1) and cytoskeletal perturbations (mTORC2) (Rispal et al., 2015; Saxton and Sabatini, 2017; Soulard et al., 2009; Wullschleger et al., 2006). A recent study (Copp et al., 2009) showed that mTOR kinase is phosphorylated differentially for mTORC1 and mTORC2: specifically mTORC1 containing mTOR phosphorylated predominantly on S2448, whereas mTORC2 contains mTOR phosphorylated predominantly on S2481. Our group has recently demonstrated the perinuclear distribution of mTORC1 (by the use of anti-mTOR phospho S2448) inside the digestive gland cells of mussels (Sforzini et al., 2018a). This study has demonstrated that even the lowest C_{60} concentration provoked a dramatic dephosphorylation of mTORC1. The results of this study indicate important linkages between mTORC1 inhibition and the alterations observed in the lysosomal system, particularly the destabilisation of the lysosomal membranes (often an indicator of induced autophagic activity), as well as the increase of L/C volume ratio that reveal excessive levels of

autophagy (i.e. catabolism of the macromolecules not compensated for by protein synthesis) (Levine and Kroemer, 2008; Moore and Viarengo, 1987; Moore et al., 2008a). The observed increase in autophagic activity was further substantiated by the enhanced expression of the LC3 protein (autophagy marker microtubule-associated protein chain 3B - LC3B), one of the most widely used biomarkers for autophagy (Fig. 3C; Chen et al., 2013; Kast and Dominguez, 2017). In addition, in the digestive gland of mussels exposed to all C_{60} concentrations, there was enhancement of lysosomal neutral lipid/triglyceride accumulation (lipidosis). This cytopathological reaction may be related to impairment of fatty acid utilization for energy generation by mitochondria, and the consequent autophagic sequestration of cytosolic lipids in the lysosomal vacuolar system (Morita et al., 2015). However, no change was observed in the lysosomal content of lipofuscins, a significant end product of oxidative attack on lipids and proteins, and a useful biomarker of moderate and severe oxidative stress (Moore, 2008; Viarengo, 1989). These results are in general agreement with previous *in vivo* studies in molluscs, demonstrating that, in organisms exposed to C_{60} under light photoperiod, oxidative stress does not appear to play a primary role in the toxicity of fullerenes at low, environmentally relevant exposures. C_{60} treatment for 24 h at 1-5 mg/L caused limited effects on lipofuscin accumulation (Canesi et al., 2010); while no change was found in lipid peroxidation levels in the digestive glands of oysters treated for 4 days with C_{60} at 1-500 μg/L (Ringwood et al., 2009). Moreover, in conjunction with the cellular data, no relevant transcriptional changes were recorded for genes involved in oxidative stress response in digestive gland cells after exposure to the three fullerene concentrations (CAT and SOD - Fig. S2, see Supplementary Information). Principal Component Analysis (PCA) is an effective method for reducing the multi-dimensionality of biomarker data and integrating this data into a "health status space" (Allen and Moore, 2004; Chatfield and Collins, 1980). Previous models have shown that there is a direct relationship between LMS, as an indicator of cellular health, and the first principal component (PC1) of other combined biomarker reactions (Allen & Moore, 2004; Moore et al., 2006; Sforzini et al., 2015,

2017, 2018a). This use of PC1 as a measure of health status space is clearly demonstrated in this work, where a strong correlation with lysosomal membrane stability is indicated (Table 1), from the correlation coefficients for the biomarkers comprising PC1 (integrated biomarker data). However, the autophagy-related biomarkers, lysosomal/cytoplasmic volume ratio and inhibition of mTORC1, were also important influences in the first principal component as an holistic indicator of cellular health, discriminating between controls and C_{60} exposed mussels (Table 1). Lysosomal lipid showed a weaker correlation (but still significant) with the first principal component (Table 1), while lipofuscin was not significantly correlated (Table 1), hence, supporting the conclusions above that oxidative stress was not significantly induced by C_{60} treatment.

The transcriptomic response showed a bell-shaped trend in the total number of genes analysed. This finding highlighted that, in the digestive gland, there was an increase of the DEGs involved in the reaction to C_{60} increasing concentrations (0.01 - 0.1 mg/L); however, at the highest concentration (1 mg/L), the transcriptomic response tended to decrease; probably related to the adverse effects of C_{60} being accumulated more rapidly. Although the number of DEGs between the lowest and highest concentration are similar, it should be noted that 0.01 mg/L C_{60} exhibited an higher number of DEGs related to energy metabolism and 1 mg/L C_{60} induced a stronger response in the DEGs related to translation and proteolysis.

The transcriptomic data may help to clarify how the digestive gland cells react to C_{60}. The results of the microarray analysis indicate that, among the DEGs involved in the energy metabolism (carbohydrate metabolism and mitochondrial activity), the higher percent is down-regulated (Table S2 - see Supplementary Information). This is the typical metabolic change associated with mTORC1 dephosphorylation, such as a reduction of the energy resources of the cells. In line with the effects of C_{60} on mTOR inhibition, it is the net increase of the up-regulated DEGs related to the lysosomal activity (Table S2). Interpretation of the biological implications of the DEGs related to protein synthesis are more difficult to explain. The DEGs involved in the translation process show

448 the maximum at the intermediate C_{60} concentration (0.1 mg/L); however, the balance between up-
449 and down-regulated genes changes in the mussels exposed to the different C_{60} concentrations, this
450 making the interpretation of the data more complicated. Nevertheless, these results show that the
451 enhanced lysosomal autophagic activity is not compensated for by a significant increase in the
452 transcription of the mRNA involved in the translation process. Furthermore, in the same animals,
453 we observed a significant increase of the L/C volume ratio: an indication that the cells had a
454 catabolic status.
455 Nanoparticles, on entry into cells, are known to induce perturbations in the cytoplasmic
456 organization; and, consequently of the cytoskeletal network (Ispanixtlahuatl-Meráz et al., 2018). In
457 previous investigations (Al-Subiai et al., 2012; Di et al., 2017), mussels exposed to C_{60} at 0.1 and 1
458 mg/L either alone or in combination with polycyclic aromatic hydrocarbons (PAHs) showed a loss
459 in definition of the digestive tubules. The phosphorylated active form of mTORC2 regulates the
460 actin cytoskeletal organization (Dobashi et al., 2011; Rispal et al., 2015). In this study, the
461 immunohistochemical fluorescent labelling of control mussel digestive gland sections by the use of
462 an anti-mTOR antibody phosphorylated on S2481 (mTORC2) highlighted an immunopositive
463 reaction, the fluorescent staining being mainly located in the cytoplasm of the tubule epithelial
464 cells: other studies (on yeast, protozoa and mammalian cells) localized mTORC2 mainly in the
465 cytoplasm (Barquilla et al., 2008; Betz and Hall, 2013; Kunz et al., 2000). Immunofluorescent
466 reaction demonstrated a strong decrease in dephosphorylated mTORC2 in mussels treated with C_{60},
467 even at the lowest fullerene concentration. This result may explain, at least in part, the pathological
468 disorganisation of the actin cytoskeleton structures observed in digestive gland tubules of C_{60}
469 exposed mussels. Microtubules, together with actin filaments and intermediate filaments, are the
470 main cytoskeletal structures in eukaryotic cells: the microtubule network is involved in various
471 physiological functions, such as cell movement, intracellular protein trafficking, and mitosis
472 (Fletcher and Mullins, 2010; Parker et al., 2014). Our immunocytochemical results showed a

striking rearrangement of the microtubular network, characterised by the presence of strongly stained tubulin containing granules in the cytoplasm (Fig. 3C & 4). The formation of granules containing tubulin has previously been demonstrated in cells from stressed organisms (Banni et al., 2016, 2017; Clark and Shay, 1981; Martin et al., 2010; Sforzini et al., 2018b). Part of the free tubulin may be also trapped on the surface of stress granules, as recently reported by Shao et al.(2017). Microtubules undergo continual disassembly and reassembly within the cell, and the synthesis of tubulin is known to be autoregulated on the basis of the amount of cytosolic unpolymerized monomer (Gasic and Mitchison, 2019). The decrease in the amount of free tubulin monomer should stimulate the protein neo synthesis in order to maintain the cytoskeletal organisation essential for cellular physiological functions such as vesicle movements and autophagy. Cytoskeletal organisation was one of the main contributing biological processes in the cytopathological reaction to fullerene as depicted by the microarray data. Tubulin was among the genes showing an increasing trend over the three C_{60} concentrations, probably to compensate for the observed alteration of this crucial cytoskeletal component of the cell.

Our data show that C_{60} accumulation in the digestive gland cells reaches a plateau in the animals treated with the lowest fullerene concentration. Actin filaments provide the mechanical capability for many cellular activities that involve membrane deformation, such as cell motility, phagocytosis, endocytosis and cytokinesis (Kast and Dominguez, 2017). mTORC2 inhibition (i.e. dephosphorylation) affects actin organisation, as well as endocytosis (Riggi et al., 2019; Rispal et al., 2015). A possible explanation of our results is that in the C_{60} treated mussels, the endocytotic (pinocytotic) uptake of nanoparticles tends to decrease, possibly related to mTORC2 dephosphorylation. Inhibition of mTORC1 also may contribute to the decrease in endocytotic capacity (Flinn & Backer, 2010).

It is also important to mention that C_{60} did not affect the overall cellular concentration of mTOR protein: the amount of the protein as well as the mRNA coding for mTOR did not show any change

498 in the animals exposed to the various fullerene concentrations. These results highlight that mTOR
499 phosphorylation / dephosphorylation mechanism is a key element in the patho-physiological
500 regulation of mussel cellular metabolism.
501

502 ## 5. Conclusions

503 In this study, we report the first published data on the subcellular distribution of C_{60} fullerene in
504 mussel digestive gland cells; and on the possible involvement of mTOR inhibition (as part of the
505 mTORC1/mTORC2 complexes) in the patho-physiological perturbations induced by nanoparticle
506 accumulation. C_{60} fullerene provokes an excessive induction of autophagy, as shown by higher
507 lysosomal activity and the enhancement of the expression of the protein LC3B; as well an increased
508 lysosomal-cytoplasmic volume ratio (L/C volume). However, no supporting evidence for C_{60}-
509 induced oxidative stress was observed, although the absence of enhanced lipofuscin does not rule
510 out the possibility of mild oxidative stress. These findings seem to indicate that moderate to severe
511 ROS production and oxidative damage are not necessary under these conditions to inhibit the
512 mTOR pathways. Autophagic induction by C_{60} (as for other nanoparticles - Stern et al., 2012;
513 Zabirnyk et al., 2007) may represent an attempted degradation in lysosomes of material that is
514 recognised by the cell as foreign or aberrant, such as pathogens or damaged intracellular proteins
515 and membranes. We have demonstrated the accumulation of C_{60} fullerene in the lysosomal-vacuolar
516 system of the major digestive gland epithelial cells (i.e. digestive cells). Excessive autophagy may
517 also be involved in the process of perturbation of cytoskeletal structures (Monastyrska et al., 2009;
518 Zheng et al., 2018). However, nanoparticles, within the cells, may themselves cause an alteration in
519 the cytoskeletal network (Ispanixtlahuatl-Meráz et al., 2018). Although the possible relationships
520 between mTORC1 and mTORC2, as well the factors that inhibit mTORC2, are not fully elucidated,
521 the cytoskeletal alterations induced by C_{60} may impair the growth of the cells and their organisation
522 in the tubules of the digestive gland. Overall, dysregulation of mTORC1 & 2 may reduce the

capacity of the cells, and organisms, to properly grow and reproduce. Consequently, mTOR dephosphorylation should be considered a diagnostic biomarker for the toxic effects of the C_{60} and polycyclic aromatic hydrocarbons as previously demonstrated (Sforzini et al., 2018a); and, under chronic stressful conditions, prognostic for potential harmful effects at the whole animal and population level. These new findings confirm and clarify why a decrease in LMS is indicative of the larger phenomenon related to mTOR inhibition that may lead to a reduction in the physiological scope for growth of the animals (Allen and Moore, 2004).

Acknowledgements

This study was supported financially by Natural Environment Research Council (NERC), UK (Grant No.NE/L006782/1; PI: ANJ).

References

Allen, J.I., Moore, M.N., 2004. Environmental prognostics: is the current use of biomarkers appropriate for environmental risk evaluation. Mar. Environ. Res. 58, 227-232.

Al-Subiai, S.N., Arlt, V.M., Frickers, P.E., Readman, J.W., Stolpe, B., Lead, J.R., Moody, A.J., Jha, A.N., 2012. Merging nano-genotoxicology with eco-genotoxicology: an integrated approach to determine interactive genotoxic and sub-lethal toxic effects of C(60) fullerenes and fluoranthene in marine mussels, *Mytilus* sp. Mutat. Res. 745, 92-103.

Banni, M., Negri, A., Mignone, F., Boussetta, H., Viarengo, A., Dondero, F., 2011. Gene expression rhythms in the mussel *Mytilus galloprovincialis* (Lam.) across an annual cycle. PLoSOne 6 (5), e18904.

545 Banni, M., Sforzini, S., Balbi, T., Corsi, I., Viarengo, A., Canesi, L., 2016. Combined effects of n-
546 TiO2 and 2,3,7,8-TCDD in *Mytilus galloprovincialis* digestive gland: a transcriptomic and
547 immunohistochemical study. Environ. Res. 145, 135-144.
548 Banni, M., Sforzini, S., Arlt, V.M., Barranger, A., Dallas, L.J., Oliveri, C., Aminot, Y., Pacchioni,
549 B., Millino, C., Lanfranchi, G., Readman, J.W., Moore, M.N., Viarengo, A., Jha, A.N., 2017.
550 Assessing the impact of Benzo[a]pyrene on Marine Mussels: Application of a novel targeted
551 low density microarray complementing classical biomarker responses. PLoS One
552 12(6):e0178460. doi: 10.1371/journal.pone.0178460.
553 Barquilla, A., Crespo, J.L., Navarro M., 2008. Rapamycin inhibits trypanosome cell growth by
554 preventing TOR complex 2 formation. Proc. Natl. Acad. Sci. USA 105, 14579-14584.
555 Barranger, A., Langan, L.M., Sharma, V., Rance, G.A., Aminot Y., Weston, N.J., Akcha, F.,
556 Moore, M.N., Arlt, V.M., Khlobystov, A.N., Readman, J.W., Jha, A.N., 2019a. Antagonistic
557 Interactions between Benzo[a]pyrene and Fullerene (C_{60}) in Toxicological Response of
558 Marine Mussels. Nanomaterials (Basel). 9(7). pii: E987. doi: 10.3390/nano9070987.
559 Barranger, A., Rance, G.A., Aminot, Y., Dallas, L.J., Sforzini, S., Weston, N.J., Banni, M., Arlt,
560 V.M., Moore, M.N., Readman, J.W., Viarengo, A., Khlobystov, A.N., Jha, A, N., 2019b. An
561 integrated approach to determine interactive genotoxic and global gene expression effects of
562 multiwalled carbon nanotubes (MWCNTs) and Benzo[a]pyrene (BaP) on marine mussels:
563 Evidence of reverse 'Trojan Horse' effects. Nanotoxicology 13, 1324-1343;
564 https://doi.org/10.1080/17435390.2019.1654003.
565 Bayne, B.L., 2009. Marine Mussels: Their Ecology and Physiology. Cambridge University Press
566 528 p.
567 Benn, T., Herckes, P., Westerhoff, P., 2012. Chapter 9 - Fullerenes in Environmental Samples: C_{60}
568 in Atmospheric Particulate Matter, in: Farré, M., Barceló, D. (Eds.), Analysis and Risk of

569 Nanomaterials in Environmental and Food Samples. Elsevier B.V., vol. 59, pp. 291-303.
570 https://doi.org/10.1016/B978-0-444-56328-6.00010-4.
571 Betz, C., Hall, M. N., 2013. Where is mTOR and what is it doing there? J. Cell Biol. 203, 563-574.
572 Bullard-Dillard, R., Creek, K.E., Scrivens, W.A., Tour, J.M., 1996. Tissue Sites of Uptake of ^{14}C-
573 Labeled C60. Bioorg. Chem. 24, 376-385.
574 Buseck, P.R., Tsipursky, S.J., Hettich, R., 1992. Fullerenes from the Geological Environment.
575 Science 257, 215-217.
576 Canesi, L., Fabbri, R., Gallo, G., Vallotto, D., Marcomini, A., Pojana, G., 2010. Biomarkers in
577 *Mytilus galloprovincialis* exposed to suspensions of selected nanoparticles (Nano carbon
578 black, C_{60} fullerene, Nano-TiO_2, Nano-SiO_2). Aquat. Toxicol. 100, 168-177.
579 Canesi, L., Ciacci, C., Fabbri, R., Marcomini, A., Pojana, G., Gallo, G., 2012. Bivalve molluscs as a
580 unique target group for nanoparticle toxicity. Mar. Environ. Res. 76, 16-21.
581 Chatfield, C., Collins, A. J., 1980. Introduction to multivariate analysis. London: Chapman and
582 Hall.
583 Chen, S., Jiang, Y.Z., Huang, L., Zhou, R.J., Yu, K.D., Liu, Y., Shao, Z.M., 2013. The residual
584 tumor autophagy marker LC3B serves as a prognostic marker in local advanced breast cancer
585 after neoadjuvant chemotherapy. Clin. Cancer Res. 19, 6853-6862.
586 Chomczynski, P., Sacchi, N., 1987. Single-step method of RNA isolation by acid guanidinium
587 thiocyanate-phenol-chloroform extraction. Anal. Biochem. 162: 156-169.
588 Clarke, K.R., 1999. Non-metric multivariate analysis in community-level ecotoxicology. Environ.
589 Toxicol. Chem. 18, 117-127.
590 Clark, M.A., Shay, J.W., 1981. The role of tubulin in the steroidogenic response of murine adrenal
591 and rat Leydig cells. Endocrinology 109, 2261-2263.
592 Clarke, K.R., Warwick, R.M., 2001. Change in marine communities: an approach to statistical
593 analysis and interpretation. PRIMER-ϵ, Plymouth, UK.

Copp, J., Manning, G., Hunter, T., 2009. TORC-specific phosphorylation of mammalian target of rapamycin (mTOR): phospho-Ser2481 is a marker for intact mTOR signaling complex 2. Cancer Res. 69, 1821-1827.

Cuervo, A.M., 2004. Autophagy: in sickness and in health. TRENDS Cell Biol. 14, 70-77.

Dallarés, S., Carrasco, N., Álvarez-Muñoz, D., Rambla-Alegre, M., Solé, M., 2018. Multibiomarker biomonitoring approach using three bivalve species in the Ebro Delta (Catalonia, Spain). Environ. Sci. Pollut. Res. Int. 25, 36745-36758.

Di, Y., Aminot, Y., Schroeder, D.C., Readman, J.W., Jha, A.N., 2017. Integrated biological responses and tissue-specific expression of *p53* and *ras* genes in marine mussels following exposure to benzo(α)pyrene and C_{60} fullerenes, either alone or in combination. Mutagenesis 32, 77-90. doi: 10.1093/mutage/gew049.

Dobashi, Y., Watanabe, Y., Miwa, C., Suzuki, S., Koyama, S., 2011. Mammalian target of rapamycin: a central node of complex signaling cascades. Int. J. Clin. Exp. Pathol. 4, 476-495.

Emke, E., Sanchís, J., Farré, M., Bäuerlein, P.S., de Voogt P., 2015. Determination of several fullerenes in sewage water by LC HR-MS using atmospheric pressure photoionization. Environ. Sci. Nano 2, 167-176.

Farré, M., Pérez, S., Gajda-Schrantz, K., Osorio, V., Kantiani, L., Ginebreda, A., Barceló, D., 2010. First determination of C_{60} and C_{70} fullerenes and N-methylfulleropyrrolidine C_{60} on the suspended material of wastewater effluents by liquid chromatography hybrid quadrupole linear ion trap tandem mass spectrometry. J. Hydrol. 383, 44-51.

Fletcher DA, Mullins RD, 2010. Cell mechanics and the cytoskeleton. Nature. 463, 485-492.

Flinn, R.J., Backer, J.M., 2010. mTORC1 signals from late endosomes: taking a TOR of the endocytic system. Cell Cycle 9, 1869-1870.

617 Franskevych, D., Palyvoda, K., Petukhov, D., Prylutska, S., Grynyuk, I., Schuetze, C., Drobot, L.,
618 Matyshevska, O., Ritter, U., 2017. Fullerene C_{60} Penetration into Leukemic Cells and Its
619 Photoinduced Cytotoxic Effects. Nanoscale Res. Lett. 12:40.
620 Gasic, I., Mitchison, T.J., 2019. Autoregulation and repair in microtubule homeostasis. Curr. Opin.
621 Cell. Biol. 56, 80-87. doi: 10.1016/j.ceb.2018.10.003.
622 Gomes, T., Pereira, C.G., Cardoso, C., Pinheiro, J.P., Cancio, I., Bebianno, M.J., 2012.
623 Accumulation and toxicity of copper oxide nanoparticles in the digestive gland of *Mytilus*
624 *galloprovincialis*. Aquat. Toxicol. 118-119, 72-79.
625 Goodarzi, S., Da Ros, T., Conde, J., Sefat, F., Mozafari, M., 2017. Fullerene: biomedical engineers
626 get to revisit an old friend. Mater. Today 20, 460-480.
627 Grebinyk, A., Grebinyk, S., Prylutska, S., Ritter, U., Matyshevska, O., Dandekar, T., Frohme, M.,
628 2018. C_{60} fullerene accumulation in human leukemic cells and perspectives of LED-mediated
629 photodynamic therapy. Free Radic. Biol. Med. 124, 319-327.
630 Huang, K., Fingar, D.C., 2014. Growing knowledge of the mTOR signaling network. Semin. Cell
631 Dev. Biol. 36, 79-90.
632 Ispanixtlahuatl-Meráz, O., Schins, R.P.F., Chirino, Y.I., 2018. Cell type specific cytoskeleton
633 disruption induced by engineered nanoparticles. Environ. Sci. Nano. 5, 228-245.
634 Kast, D.J., Dominguez, R., 2017. The Cytoskeleton-Autophagy Connection. Curr. Biol. 27, R318-
635 R326.
636 Khan, I., Saeed, K., Khan, I., 2017. Nanoparticles: Properties, applications and toxicities. Arab. J.
637 Chem., Available online 18 May 2017. https://doi.org/10.1016/j.arabjc.2017.05.011.
638 Klionsky, D. J., Emr, S. D., 2000. Autophagy as a regulated pathway of cellular degradation.
639 Science 290, 1717-1721.
640 Krusic, P.J., Wasserman, E., Keizer, P.N., Morton, J.R., Preston, K.F., 1991. Radical reactions of
641 c60. Science 254, 1183-1185.

642 Kunz, J., Schneider, U., Howald, I., Schmidt, A., Hall, M.N., 2000. HEAT repeats mediate plasma
643 membrane localization of Tor2p in yeast. J. Biol. Chem. 275, 37011-37020.
644 Levine, B., Kroemer, G., 2008. Autophagy in the pathogenesis of disease. Cell. 132, 27-42.
645 Liu, Q., Cui, Q., Li, X.J., Jin, L., 2014. The applications of buckminsterfullerene C_{60} and
646 derivatives in orthopaedic research. Connect. Tissue Res. 55, 71-79.
647 Maisano, M., Cappello, T., Natalotto, A., Vitale, V., Parrino, V., Giannetto, A., Oliva, S., Mancini,
648 G., Cappello, S., Mauceri, A., Fasulo, S., 2017. Effects of petrochemical contamination on
649 caged marine mussels using a multi-biomarker approach: Histological changes, neurotoxicity
650 and hypoxic stress. Mar. Environ. Res. 128, 114-123.
651 Martin, D., Duarte, M., Lepault, J., Poncet, D., 2010. Sequestration of free tubulin molecules by the
652 viral protein NSP2 induces microtubule depolymerisation during rotavirus infection. J. Virol.
653 84, 2522-2532.
654 McCarthy, M.P., Carroll, D.L., Ringwood, A.H., 2013. Tissue specific responses of oysters,
655 *Crassostrea virginica*, to silver nanoparticles. Aquat. Toxicol. 138-139, 123-128.
656 Monastyrska, I., Rieter, E., Klionsky, D.J., Reggiori, F., 2009. Multiple roles of the cytoskeleton in
657 autophagy. Biol. Rev. Camb. Philos. Soc. 84, 431-448.
658 Moore, M.N., 1976. Cytochemical demonstration of latency of lysosomal hydrolases in digestive
659 gland cells of the common mussel *Mytilus edulis*, and changes induced by thermal stress. Cell
660 Tissue Res. 175, 279-287.
661 Moore, M.N., 1988. Cytochemical responses of the lysosomal system and NADPH-
662 ferrihemoprotein reductase in molluscan digestive cells to environmental and experimental
663 exposure to xenobiotics. Mar. Ecol. Prog. Ser. 46, 81-89.
664 Moore, M.N., 2008. Autophagy as a second level protective process in conferring resistance to
665 environmentally-induced oxidative stress. Autophagy 4, 254-256.

666 Moore, M.N., 2010. Is toxicological pathology characterised by a loss of system complexity? Mar.
667 Environ. Res. 69, S37-S41.
668 Moore, M.N., Clarke, K.R., 1982. Use of microstereology and cytochemical staining to determine
669 the effects of crude oil-derived aromatic hydrocarbons on lysosomal structure and function in
670 a marine bivalve mollusc *Mytilus edulis*. Histochem. J. 14, 713-718.
671 Moore, M.N., Viarengo, A., 1987. Lysosomal membrane fragility and catabolism of cytosolic
672 proteins: evidence for a direct relationship. Experientia 43, 320-323.
673 Moore, M.N., Allen, J.I., McVeigh, A., 2006. Environmental prognostics: an integrated model
674 supporting lysosomal stress responses as predictive biomarkers of animal health status. Mar.
675 Environ. Res., 61, 278-304.
676 Moore, M.N., Viarengo, A., Donkin, P., Hawkins, A.J., 2007. Autophagic and lysosomal reactions
677 to stress in the hepatopancreas of blue mussels. Aquat. Toxicol. 84, 80-91.
678 Moore, M.N., Koehler, A., Lowe, D., Viarengo, A., 2008. Lysosomes and autophagy in aquatic
679 animals, in: Klionsky, D. (Ed.), Methods in Enzymology. Academic Press/Elsevier,
680 Burlington, pp. 582-620.
681 Moore, M.N., Readman, J.A.J., Readman, J.W., Lowe, D.M., Frickers, P.E., Beesley, A., 2009.
682 Lysosomal cytotoxicity of carbon nanoparticles in cells of the molluscan immune system: an
683 *in vitro* study. Nanotoxicology 3, 40-45.
684 Moore, M.N., Shaw, J.P., Ferrar Adams, D.R., Viarengo, A., 2015. Anti-oxidative cellular
685 protection effect of fasting-induced autophagy as a mechanism for hormesis. Mar. Environ.
686 Res. 107, 35-44.
687 Morita, M., Gravel, S.P., Hulea, L., Larsson, O., Pollak, M., St-Pierre, J., Topisirovic, I., 2015.
688 mTOR coordinates protein synthesis, mitochondrial activity and proliferation. Cell Cycle 14,
689 473-480.

690 Negri, A., Oliveri, C., Sforzini, S., Mignione, F., Viarengo, A., Banni, M., 2013. Transcriptional
691 response of the mussel *Mytilus galloprovincialis* (Lam.) following exposure to heat stress and
692 copper. PLoS One 8(6):e66802.
693 Nielsen, G.D., Roursgaard, M., Jensen, K.A., Poulsen, S.S., Larsen, S.T. 2008. *In vivo* biology and
694 toxicology of fullerenes and their derivatives. Basic Clin. Pharmacol. Toxicol. 103, 197-208.
695 Oberdörster, E., 2004. Manufactured nanomaterials (fullerenes, C_{60}) induce oxidative stress in the
696 brain of juvenile largemouth bass. Environ. Health Perspect. 112, 1058-1062.
697 Oberdörster, E., Zhu, S., Blickley, T.M., McClellan-Green, P., Haasch, M.L., 2006. Ecotoxicology
698 of carbon-based engineered nanoparticles: Effects of fullerene (C_{60}) on aquatic organisms.
699 Carbon 44, 1112-1120.
700 Parker, A.L., Kavallaris, M., McCarroll, J.A., 2014. Microtubules and their role in cellular stress in
701 cancer. Front. Oncol. 4, 153.
702 Pearse, A.G.E., 1972, third ed. Histochemistry Theoretical and Applied, vol. 2 Churchill
703 Livingstone, Edinburgh and London. 1518 pp.
704 Pfaffl, M.W., Horgan, G.W., Dempfle, L., 2002. Relative expression software tool (REST©) for
705 group-wise comparison and statistical analysis of relative expression results in real-time PCR.
706 Nucleic Acids Res. 30: e36.
707 Phillips, S.N., Muzaffar, N., Codlin, S., Korey, C.A., Taschner, P.E., de Voer, G., Mole, S.E.,
708 Pearce, D.A., 2006. Characterizing pathogenic processes in Batten disease: use of small
709 eukaryotic model systems. Biochim. Biophys. Acta 1762, 906-919.
710 Porter, A.E., Gass, M., Muller, K., Skepper, J.N., Midgley, P., Welland, M., 2007. Visualizing the
711 uptake of C_{60} to the cytoplasm and nucleus of human monocyte-derived macrophage cells
712 using energy-filtered transmission electron microscopy and electron tomography. Environ.
713 Sci. Technol. 41, 3012-3017.

714 Pycke, B.F., Chao, T.C., Herckes, P., Westerhoff, P., Halden, R.U., 2012. Beyond nC60: strategies
715 for identification of transformation products of fullerene oxidation in aquatic and biological
716 samples. Anal. Bioanal. Chem. 404, 2583-2595.
717 Raoof, M., Mackeyev, Y., Cheney, M.A., Wilson, L.J., Curley, S.A., 2012. Internalization of C_{60}
718 fullerenes into cancer cells with accumulation in the nucleus via the nuclear pore complex.
719 Biomaterials 33, 2952-2960.
720 Riggi, M., Bourgoint, C., Macchione, M., Matile, S., Loewith, R., Roux, A., 2019. TORC2 controls
721 endocytosis through plasma membrane tension. J. Cell Biol. 218, 2265.
722 Ringwood, A.H., Levi Polyachenko, N., Carroll, D.L., 2009. Fullerene exposures with oysters:
723 embryonic, adult, and cellular responses. Environ. Sci. Technol. 43, 7136-7141.
724 Rispal, D., Eltschinger, S., Stahl, M., Vaga, S., Bodenmiller, B., Abraham, Y., Filipuzzi, I., Movva,
725 N.R., Aebersold, R., Helliwell, S.B., Loewith, R., 2015. Target of Rapamycin Complex 2
726 Regulates Actin Polarization and Endocytosis via Multiple Pathways. J. Biol. Chem. 290,
727 14963-14978.
728 Russ, K.A., Elvati, P., Parsonage, T.L., Dews, A., Jarvis, J.A., Ray, M., Schneider, B., Smith, P.J.,
729 Williamson, P.T., Violi, A., Philbert, M.A., 2016. C_{60} fullerene localization and membrane
730 interactions in RAW 264.7 immortalized mouse macrophages. Nanoscale 8, 4134-4144.
731 Sanchís, J., Berrojalbiz, N., Caballero, G., Dachs, J., Farré, M., Barceló, D., 2012. Occurrence of
732 Aerosol-Bound Fullerenes in the Mediterranean Sea Atmosphere. Environ. Sci. Technol 46,
733 1335-1343. DOI: 10.1021/es200758m.
734 Sanchís, J., Božović, D., Al-Harb,i N.A., Silva, L.F., Farré, M., Barceló, D., 2013. Quantitative
735 trace analysis of fullerenes in river sediment from Spain and soils from Saudi Arabia. Anal.
736 Bioanal. Chem. 405, 5915-5923. doi: 10.1007/s00216-013-6924-z.
737 Sanchís, J., Oliveira, L.F., de Leão, F.B., Farré, M., Barceló, D., 2015. Liquid chromatography-
738 atmospheric pressure photoionization-Orbitrap analysis of fullerene aggregates on surface

739 soils and river sediments from Santa Catarina (Brazil). Sci Total Environ. 505, 172-179. doi:
740 10.1016/j.scitotenv.2014.10.006.
741 Sanchís, J., Llorca, M., Olmos, M., Schirinzi, G.F., Bosch-Orea, C., Abad, E., Barceló, D., Farré,
742 M., 2018. Metabolic Responses of *Mytilus galloprovincialis* to Fullerenes in Mesocosm
743 Exposure Experiments. Environ. Sci. Technol. 52, 1002-1013.
744 Saxton, R.A., Sabatini, D.M., 2017. mTOR Signaling in Growth, Metabolism, and Disease. Cell.
745 168, 960-976.
746 Sforzini, S., Moore, M.N., Boeri, M., Benfenati, E., Colombo, A., Viarengo, A., 2014.
747 Immunofluorescence detection and localization of B[*a*]P and TCDD in earthworm tissues.
748 Chemosphere 107, 282-289.
749 Sforzini, S., Moore, M.N., Boeri, M., Bencivenga, M., Viarengo, A., 2015. Effects of PAHs and
750 dioxins on the earthworm *Eisenia andrei*: A multivariate approach for biomarker
751 interpretation. Environ. Pollut. 196, 60-71.
752 Sforzini, S., Moore, M., Mou, Z., Boeri, M., Banni, M., Viarengo, A., 2017. Mode of action of
753 Cr(VI) in immunocytes of earthworms: implications for animal health. Ecotoxicol. Environ.
754 Saf. 138, 298-308.
755 Sforzini, S., Moore, M.N., Oliveri, C., Volta, A., Jha, A., Banni, M., Viarengo, A., 2018a. Role of
756 mTOR in autophagic and lysosomal reactions to environmental stressors in molluscs. Aquat.
757 Toxicol. 195, 114-128.
758 Sforzini, S., Oliveri, C., Orrù, A., Chessa, G., Jha, A., Viarengo, A., Banni, M., 2018b. Application
759 of a new targeted low density microarray and conventional biomarkers to evaluate the health
760 status of marine mussels: A field study in Sardinian coast, Italy. Sci. Total Environ. 628-629,
761 319-328.

762 Shao, J., Gao, F., Zhang, B., Zhao, M., Zhou, Y., He, J., Ren, L., Yao, Z., Yang, J., Su, C., Gao, X.,
763 2017. Aggregation of SND1 in Stress Granules is Associated with the Microtubule
764 Cytoskeleton During Heat Shock Stimulus. Anat. Rec. (Hoboken) 300, 2192-2199.
765 Soulard, A., Cohen, A., Hall, M.N., 2009. TOR signaling in invertebrates. Curr. Opin. Cell Biol. 21,
766 825-836.
767 Stern, S.T., Adiseshaiah, P.P., Crist, R.M., 2012. Autophagy and lysosomal dysfunction as
768 emerging mechanisms of nanomaterial toxicity. Part. Fibre Toxicol. 9, 20.
769 Sumner, S.C., Snyder, R.W., Wingard, C., Mortensen, N.P., Holland, N.A., Shannahan, J.H.,
770 Dhungana, S., Pathmasiri, W., Han, L., Lewin, A.H., Fennell, T.R., 2015. Distribution and
771 biomarkers of carbon-14 labeled fullerene C_{60} ($[^{14}C(U)]C_{60}$) in female rats and mice for up to
772 30 days after intravenous exposure. J. Appl. Toxicol. 35, 1452-1464.
773 Tedesco, S., Doyle, H., Blasco, J., Redmond, G., Sheehan, D., 2010. Oxidative stress and toxicity of
774 gold nanoparticles in *Mytilus edulis*. Aquat Toxicol. 100, 178-186.
775 Tervonen, K., Waissi, G., Petersen, E.J., Akkanen, J., Kukkonen, J.V., 2010. Analysis of fullerene-
776 C_{60} and kinetic measurements for its accumulation and depuration in *Daphnia magna*.
777 Environ. Toxicol. Chem. 29, 1072-1078.
778 Trpkovic, A., Todorovic-Markovic, B., Trajkovic, V., 2012. Toxicity of pristine versus
779 functionalized fullerenes: mechanisms of cell damage and the role of oxidative stress. Arch.
780 Toxicol. 86, 1809-1827.
781 Urbaszek, P., Gajewicz, A., Sikorska, C., Haranczyk, M., Puzyn, T., 2017. Modeling adsorption of
782 brominated, chlorinated and mixed bromo/chloro-dibenzo-*p*-dioxins on C_{60} fullerene using
783 Nano-QSPR. Beilstein J. Nanotechnol 8, 752-761.
784 Viarengo, A., 1989. Heavy metals in marine invertebrates: mechanisms of regulation and toxicity at
785 the cellular level. Rev. Aquat. Sci. 1, 295-317.

Viarengo, A., Zanicchi, G., Moore, M.N., Orunesu, M., 1981. Accumulation and detoxication of copper by the mussel *Mytilus galloprovincialis* Lam.: A study of the subcellular distribution in the digestive gland cells. Aquat. Toxicol. 1, 147–157.

Viarengo, A., Lowe, D., Bolognesi, C., Fabbri, E., Koehler, A., 2007. The use of biomarkers in biomonitoring: a 2-tier approach assessing the level of pollutant-induced stress syndrome in sentinel organisms. Comp. Biochem. Physiol. C 146, 281-300.

Wullschleger, S., Loewith, R., Hall, M.N., 2006. TOR signaling in growth and metabolism. Cell 124, 471-484.

Zabirnyk, O., Yezhelyev, M., Seleverstov, O., 2007. Nanoparticles as a novel class of autophagy activators. Autophagy 3, 278-281.

Zheng, W., Wang, B., Si, M., Zou, H., Song, R., Gu, J., Yuan, Y., Liu, X., Zhu, G., Bai, J., Bian, J., Liu, Z., 2018. Zearalenone altered the cytoskeletal structure via ER stress-autophagy-oxidative stress pathway in mouse TM4 Sertoli cells. Sci. Rep. 8, 3320.

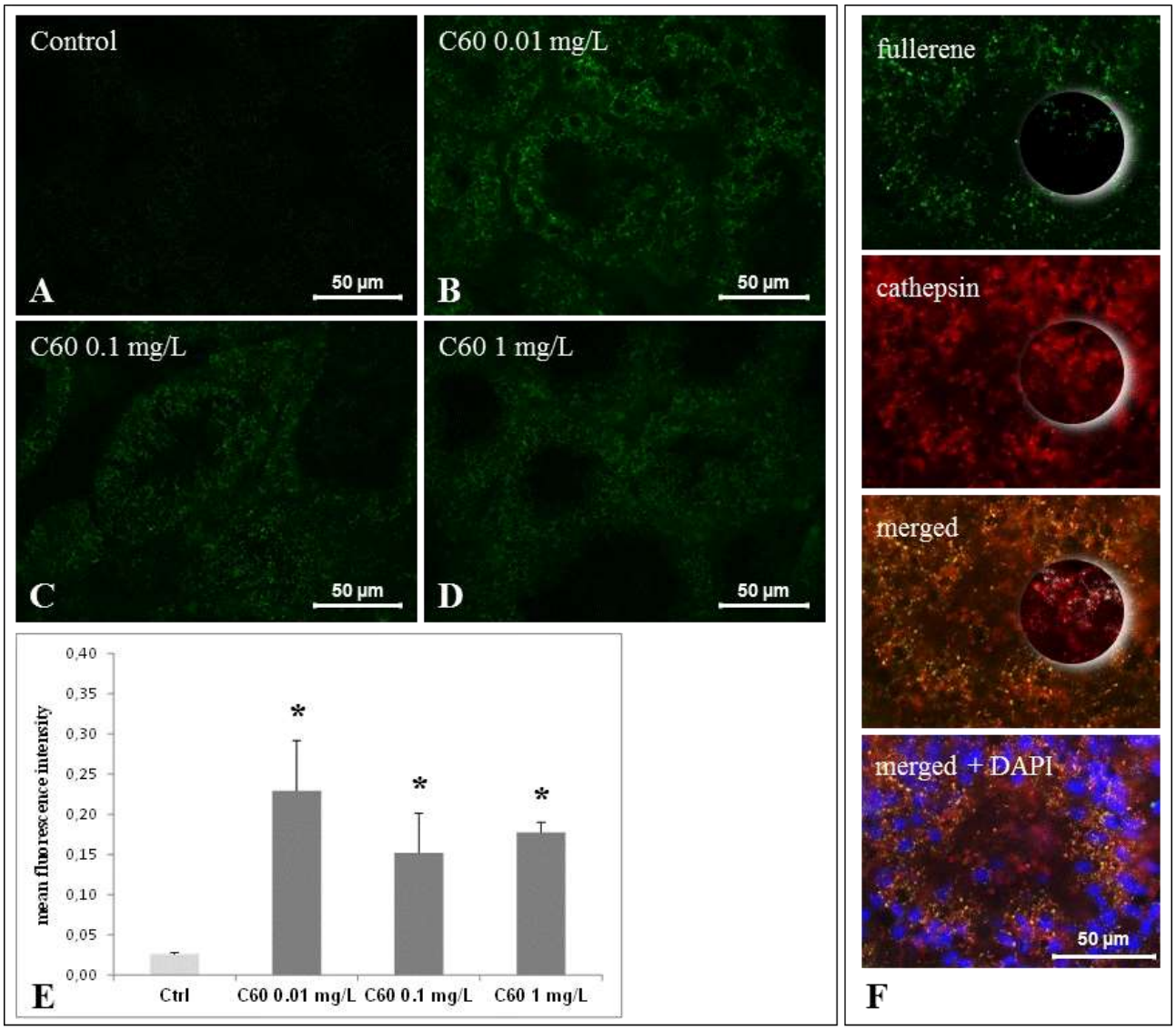

800

801 Fig. 1.

802

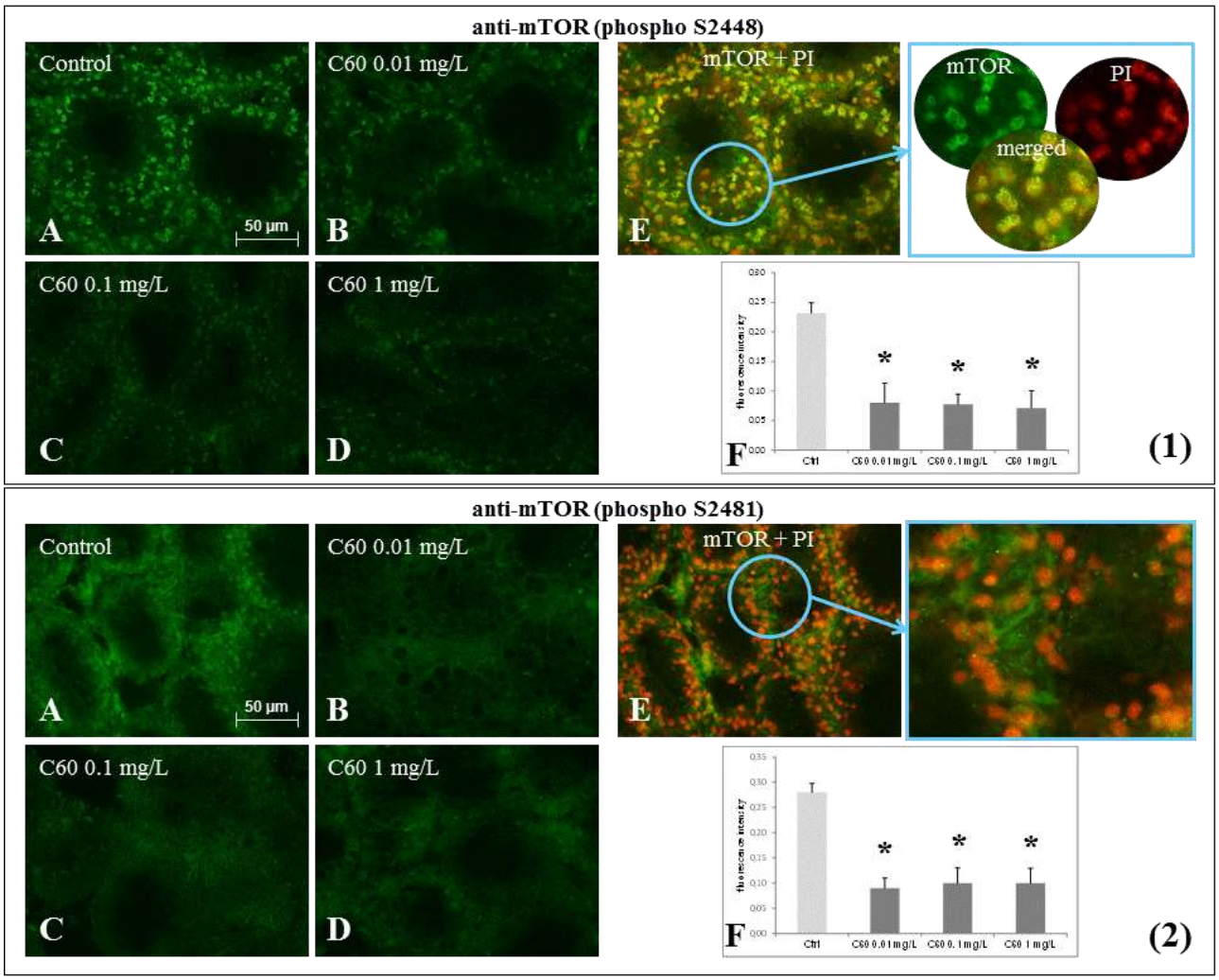

803

804 Fig. 2.

805

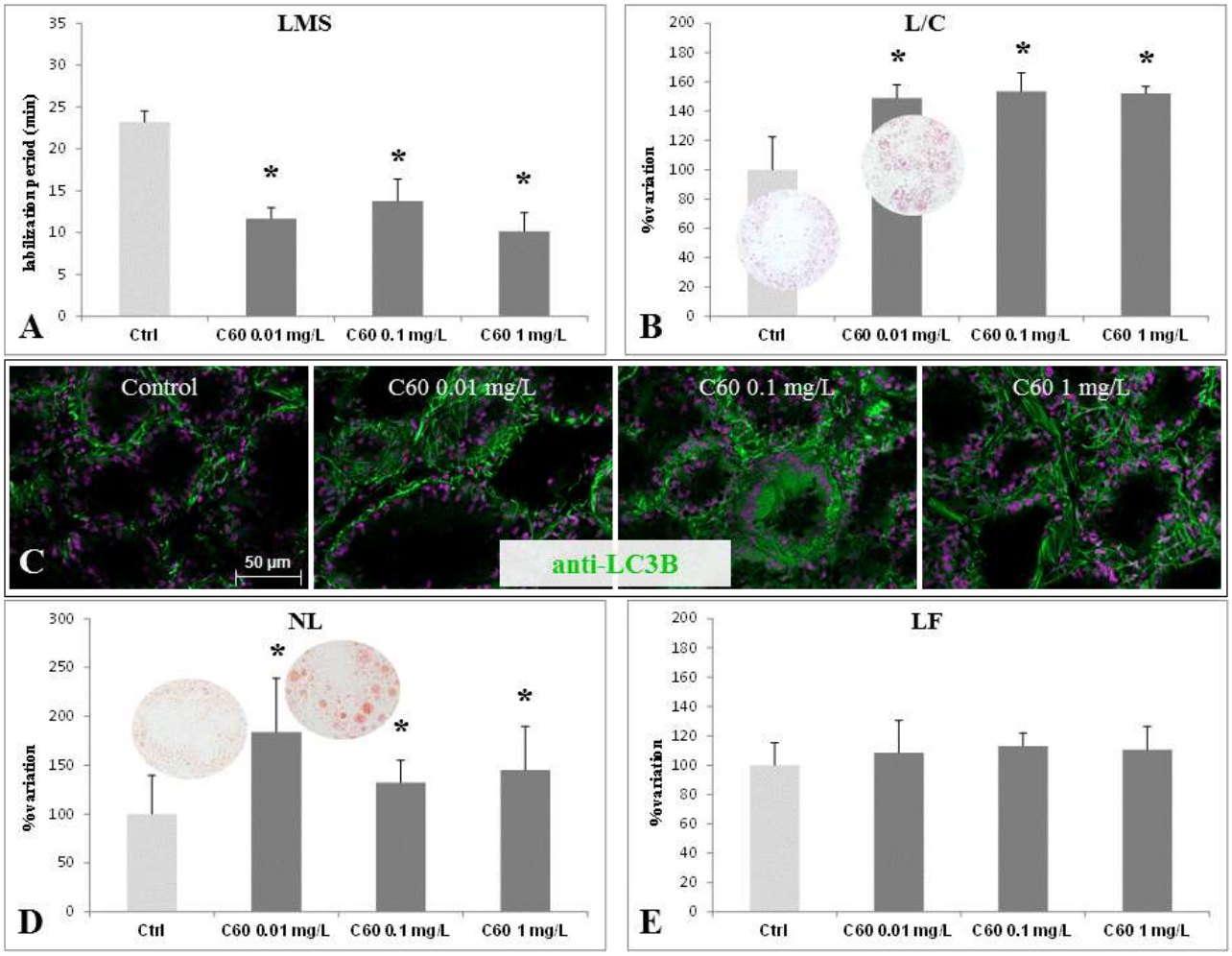

806

807 Fig. 3.

808

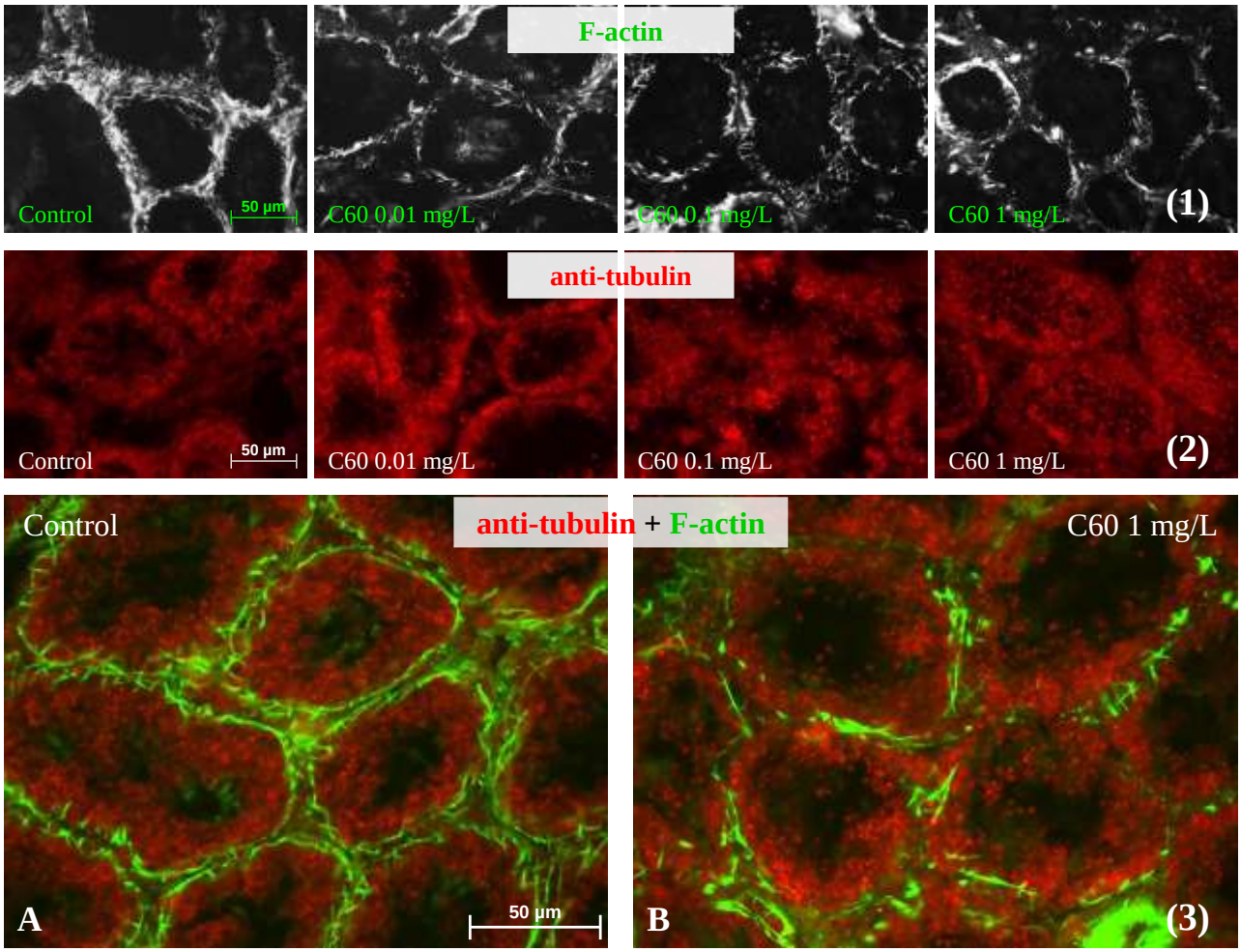

809

810 Fig. 4.

811

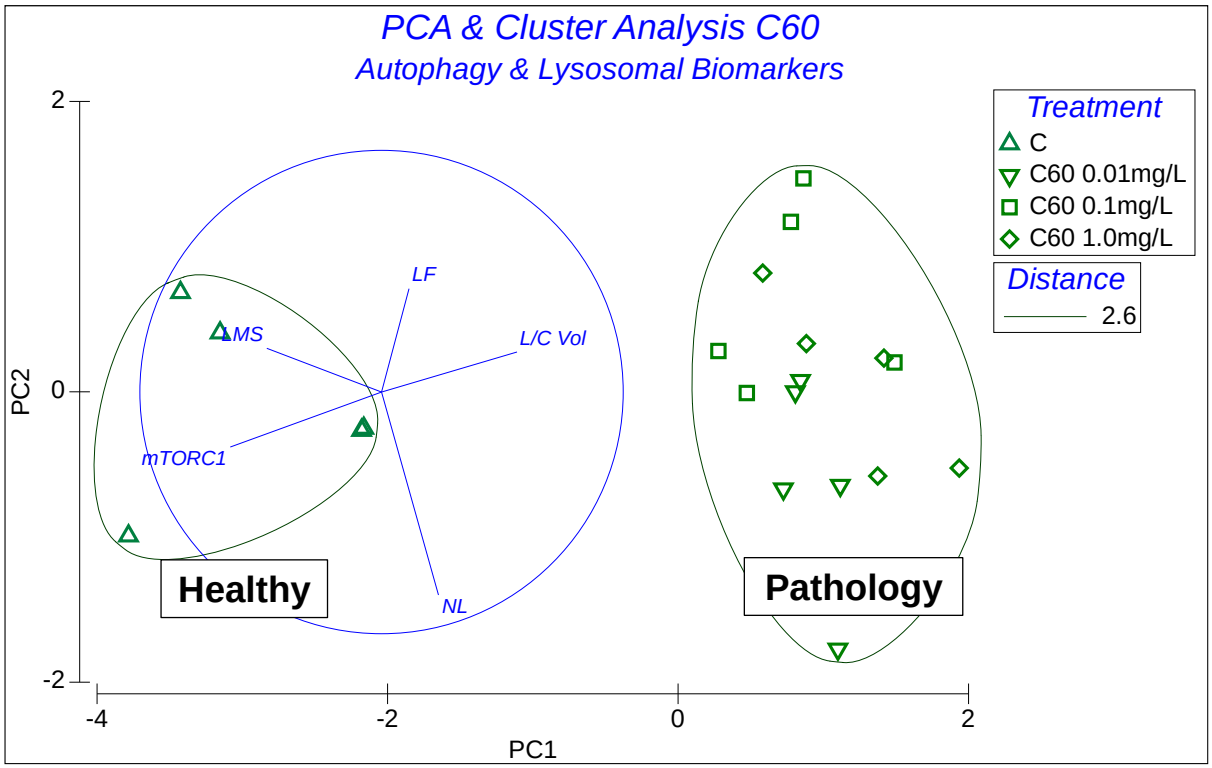
PCA & Cluster Analysis C60
Autophagy & Lysosomal Biomarkers
Treatment
C
C60 0.01mg/L
C60 0.1mg/L
C60 1.0mg/L
Distance
2.6
LF
AMS
L/C Vol
mTORC1
NL
Healthy
Pathology
PC2
PC1
2
0
-2
-4
-2
0
2

Fig. 5.

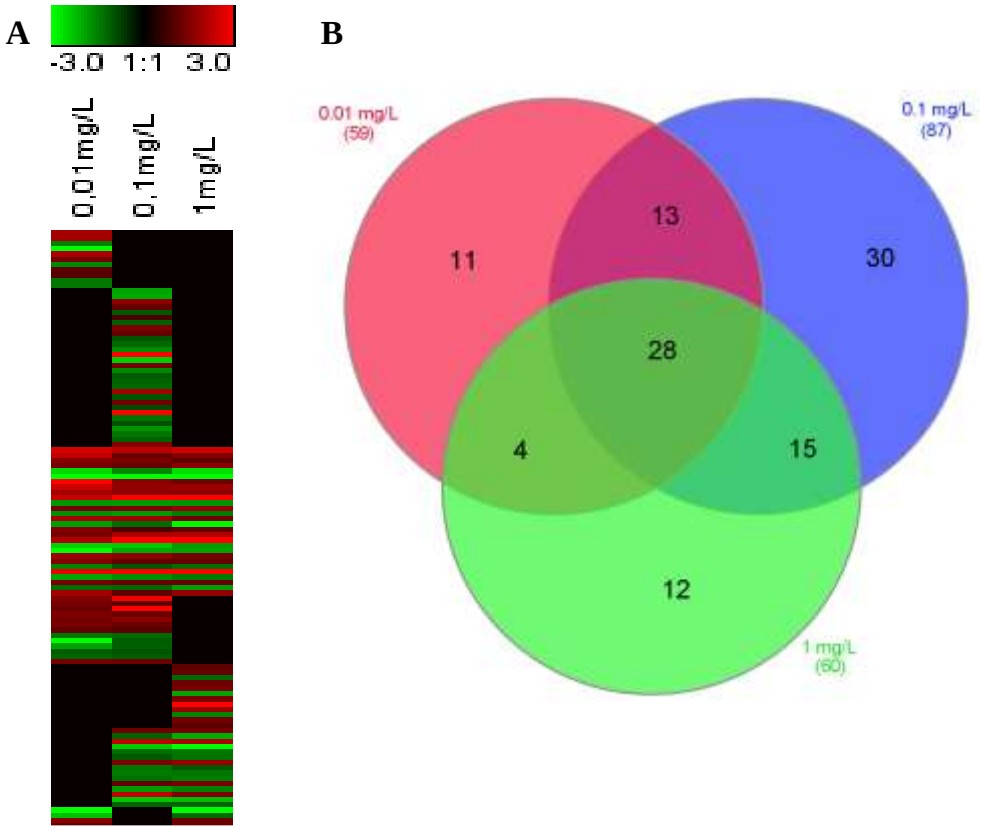

815

816 Fig. 6.

817

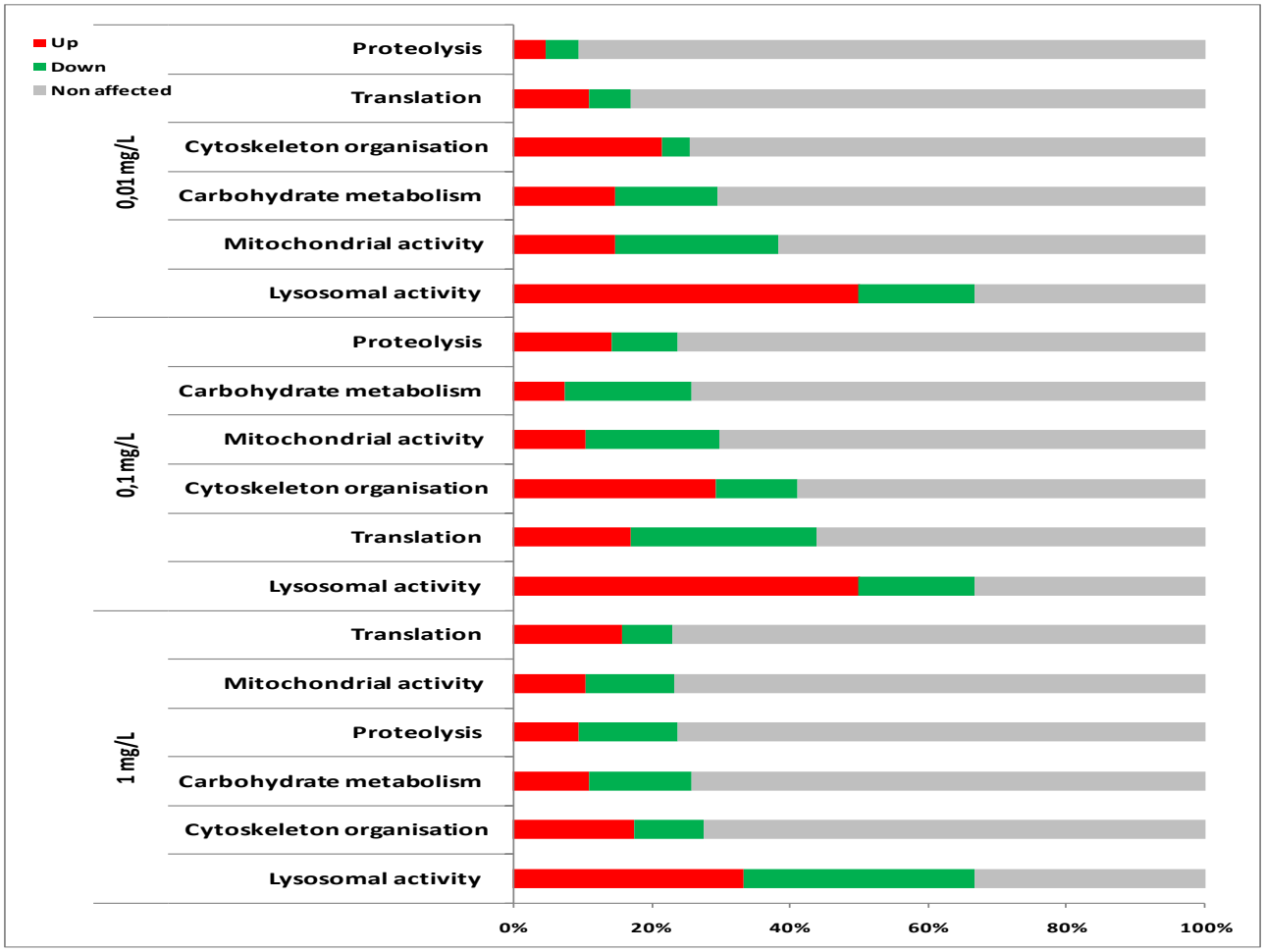

818

819 Fig. 7.

820

Fig. 1. Anti-C_{60} Fullerene immunohistochemical staining (green: FITC conjugated secondary antibody) of digestive gland tissue sections from mussels exposed to different experimental conditions (A: Control; B: 0.01 mg/L C_{60}; C: 0.1 mg/L C_{60}; D: 1 mg/L C_{60}). E) Quantitative fluorescence analysis of anti-C_{60} immunoreaction. Data are mean ± SD of at least five replicates; * = $p < 0.05$ (Mann-Whitney *U*-test). F) Double immunohistochemical staining of digestive glands from mussels exposed to 0.01 mg/L C_{60} fullerene with anti-C_{60} and -cathepsin D antibodies (separate colour images for fullerene (FITC, green) and cathepsin D (DyLight594, red) immunoreactivity were merged into a composite image, whereby the colocalization of both antigens resulted in a yellow colour); in the last picture, nuclei were stained with DAPI (blue).

Fig. 2. Anti-mTOR phospho S2448 (mTORC1) (Panel 1) and anti-mTOR phospho S2481 (mTORC2) (Panel 2) immunohistochemical staining (green: Chromeo conjugated secondary antibody) of digestive gland tissue sections from mussels exposed to different experimental conditions (A: Control; B: 0.01 mg/L C_{60}; C: 0.1 mg/L C_{60}; D: 1 mg/L C_{60}). E) Anti-phospho mTOR (green: Chromeo) and propidium iodide (PI, red) double staining in sections of digestive glands from control mussels. (Panel 1) the anti-mTOR phospho S2448 (mTORC1) fluorescence is located mainly in the perinuclear region of the tubule epithelial cells (yellow colour in the composite image); (Panel 2) the anti-mTOR phospho S2481 (mTORC2) fluorescence is located in the cytoplasm. F) Quantitative fluorescence analysis of anti-mTORC1 (Panel 1) and anti-mTORC2 (Panel 2) immunoreaction. Data are mean ± SD of at least five replicates; * = $p < 0.05$ (Mann-Whitney *U*-test).

Fig. 3. Lysosomal responses in digestive gland of mussels exposed to C_{60} (0.01, 0.1, 1 mg/L): A) Lysosomal membrane stability (LMS); B) lysosomal/cytoplasmic volume ratio (L/C); C) anti-LC3B immunohistochemical staining (green: Alexa Fluor® 488 conjugated secondary antibody; violet:

DAPI nuclear staining; D) neutral lipid accumulation (NL); E) lipofuscin content (LF). Data represent the mean ± SD of at least five replicates. * indicates statistically significant differences ($p < 0.05$ Mann-Whitney *U*-test).

Fig. 4. (Panel 1) F-actin cytoskeleton fluorescent staining by Green Fluorescent Phalloidin Conjugate (greyscale images) and (Panel 2) immunofluorescent anti-tubulin staining (red: DyLight® 594 conjugated secondary antibody) of digestive gland tissue sections from mussels exposed to different experimental conditions (Control, C_{60} 0.01 mg/L, C_{60} 0.1 mg/l, C_{60} 1 mg/L); (Panel 3) antibody to tubulin (red) and F-actin (green) combination staining of tissues sections of Controls (A) and C_{60} 1 mg/L exposed mussels (B).

Fig. 5. Principal component and cluster analysis for the five autophagy/lysosomal function related biomarkers. Vectors are shown for lysosomal membrane stability (LMS), lipofuscin (LF), lysosomal triglyceride (NL), active form (phosphorylated) of the mechanistic target for rapamycin complex 1 cell signalling system (p-mTORC1), and lysosomal/cytoplasmic volume ratio (L/C Vol). Healthy and diseased (pathology) regions of the "health status space" are indicated. PC1 captured 69.6% of the variation.

Fig. 6. Digestive gland expression level profiles of mussels exposed to three increasing concentrations of C_{60} fullerene against controls. A) The heat map (Pearson correlation, complete linkage algorithm) reports the log2 relative expression level with respect to reference condition. 113 differentially expressed genes were generated in at least one condition. B) Venn diagram representation of gene expression patterns clearly depicted that 28 differentially expressed genes (DEGs) are shared between the three species. All DEGs are obtained with respect to the control

870 condition. Data used to create the Venn-diagram were obtained from microarray analysis. Four
871 biological replicates were considered.
872
873 Fig. 7. Over-representation analysis of DEGs in the digestive gland of mussels exposed to C_{60} (0.01
874 mg/L, 0.1 mg/L and 1 mg/L). Showed are: experimental conditions; biological processes;
875 percentage of up- and down-regulated genes. The over-represented biological processes in C_{60}
876 exposed animals versus control.